RESEARCH ARTICLE

JBMR®

Subcanalicular Nanochannel Volume Is Inversely Correlated With Calcium Content in Human Cortical Bone

Tengteng Tang,[1] William Landis,[2] Stéphane Blouin,[3] Luca Bertinetti,[4] Markus A. Hartmann,[3] Andrea Berzlanovich,[5] Richard Weinkamer,[1] Wolfgang Wagermaier,[1] and Peter Fratzl[1]

[1]Department of Biomaterials, Max Planck Institute of Colloids and Interfaces, Potsdam, Germany
[2]Department of Preventive and Restorative Dental Sciences, University of California at San Francisco, San Francisco, CA, USA
[3]Ludwig Boltzmann Institute of Osteology at Hanusch Hospital of OEGK and AUVA Trauma Centre Meidling, 1st Med. Department Hanusch Hospital, Vienna, Austria
[4]Center for Molecular Bioengineering, TU Dresden, Dresden, Germany
[5]Center of Forensics Medicine, Medical University of Vienna, Vienna, Austria

ABSTRACT

The spatial distribution of mineralization density is an important signature of bone growth and remodeling processes, and its alterations are often related to disease. The extracellular matrix of some vertebrate mineralized tissues is known to be perfused by a lacunocanalicular network (LCN), a fluid-filled unmineralized structure that harbors osteocytes and their fine processes and transports extracellular fluid and its constituents. The current report provides evidence for structural and compositional heterogeneity at an even smaller, subcanalicular scale. The work reveals an extensive unmineralized three-dimensional (3D) network of nanochannels (~30 nm in diameter) penetrating the mineralized extracellular matrix of human femoral cortical bone and encompassing a greater volume fraction and surface area than these same parameters of the canaliculi comprising the LCN. The present study combines high-resolution focused ion beam-scanning electron microscopy (FIB-SEM) to investigate bone ultrastructure in 3D with quantitative backscattered electron imaging (qBEI) to estimate local bone mineral content. The presence of nanochannels has been found to impact qBEI measurements fundamentally, such that volume percentage (vol%) of nanochannels correlates inversely with weight percentage (wt%) of calcium. This mathematical relationship between nanochannel vol% and calcium wt% suggests that the nanochannels could potentially provide space for ion and small molecule transport throughout the bone matrix. Collectively, these data propose a reinterpretation of qBEI measurements, accounting for nanochannel presence in human bone tissue in addition to collagen and mineral. Further, the results yield insight into bone mineralization processes at the nanometer scale and present the possibility for a potential role of the nanochannel system in permitting ion and small molecule diffusion throughout the extracellular matrix. Such a possible function could thereby lead to the sequestration or occlusion of the ions and small molecules within the extracellular matrix. © 2022 The Authors. *Journal of Bone and Mineral Research* published by Wiley Periodicals LLC on behalf of American Society for Bone and Mineral Research (ASBMR).

KEY WORDS: HUMAN BONE; BIOMINERALIZATION; NANOCHANNELS; QUANTITATIVE BACKSCATTERED ELECTRON IMAGING; FOCUSED ION BEAM-SCANNING ELECTRON MICROSCOPY

Introduction

Human cortical bone may be considered as a nanofibrous composite with a complex hierarchical structure that is principally comprised of protein (mainly type I collagen), mineral (hydroxyapatite), and water.[1-3] The mineral content varies in bone as a result of two processes, mineralization and remodeling.[3,4] These two dynamic processes are effectively orchestrated by bone cells, in particular osteocytes, through mechanosensing[5] that allows bone to adapt to different biological and mechanical demands. Further, human bone is a major reservoir for mineral as it contains more than 90% of the calcium in the human body.[6] A lacunocanalicular network (LCN), a system that hosts osteocytes and their cytoplasmic processes and consists of osteocyte lacunae interconnected by nanometer-sized channels (canaliculi), is well known for its essential role in

Received in original form June 27, 2022; revised form November 10, 2022; accepted November 23, 2022.
Address correspondence to: Peter Fratzl, PhD, Department of Biomaterials, Max Planck Institute of Colloids and Interfaces, Am Mühlenberg 1, 14476 Potsdam, Germany. Email: peter.fratzl@mpikg.mpg.de
Additional Supporting Information may be found in the online version of this article.
Journal of Bone and Mineral Research, Vol. 38, No. 2, February 2023, pp 313–325.
DOI: 10.1002/jbmr.4753

facilitating mechanotransduction,[7,8] mineral homeostasis through perilacunar/canalicular remodeling,[9] and fluid and solute transport.[5,10] These characteristics of the LCN have been deduced in part from numerous electron microscopic, X-ray nanotomographic and confocal laser scanning microscopic, as well as other imaging techniques.[11-14]

Recent advances in three-dimensional (3D) imaging of biomineralized tissues have enabled visualization of fine ultrastructural features in mineralizing turkey leg tendon,[15,16] mouse bone and calcified cartilage,[17] and human bone[18,19] beyond the ~100 nm length scales of the LCN. 3D focused ion beam-scanning electron microscopy (FIB-SEM) studies in turkey leg tendon and mouse bone and cartilage have described the existence of a subcanalicular or nanochannel network that is much more extensive than the LCN and may provide additional and complementary pathways for mineral ion and/or mineral precursor transport.[15,17] The presence of such a nanochannel network within the extracellular matrix of the mineralized tissue may have implications in mineral homeostasis. The LCN volume and surface area have implications for bone mineralization as they provide extracellular matrix access to ions and small molecules.[20] 3D imaging of the bone LCN using synchrotron radiation phase-contrast nano-CT[21,22] and confocal microscopy[23] has revealed that 50% of the mineralized tissue in the human skeleton is located within ~1.5 μm of the closest LCN boundary and 80% within 2 to 3 μm. Further, a recent FIB-SEM examination of forming human bone suggests co-diffusion of mineralization precursors, promotors, and inhibitors from the LCN to the bone matrix,[24] an observation highlighting the role of the LCN in supporting and achieving mineral homeostasis. Given the recent discovery of nanochannels in avian tendon[15] and murine bone and calcified cartilage[17] mentioned above, the current study has examined human cortical bone ultrastructure to identify the possible presence of nanochannels in this tissue and, in particular, their structural or architectural properties such as volume fraction and surface area in comparison to those of the LCN.

In a related context, bone tissue is known to be heterogeneous in mineral content (mass/density and location/distribution) across its structural hierarchy,[25,26] a feature that principally results from bone turnover and the mineralization kinetics of the tissue.[27,28] One of the most well established and readily available methods for characterizing bone mineral heterogeneity at a microscopic level is quantitative backscattered electron imaging (qBEI), a technique first proposed and applied by Boyde and colleagues[29] and elaborated by Roschger and colleagues.[30] qBEI relies on the principle that the signal intensity/gray level under backscattered electron imaging (that is, the number of backscattered electrons) is linearly proportional to the local average atomic number, Z, of the specimen within the tissue volume probed by the electron beam. As such, regions of high average atomic number/high mineral content appear brighter (higher gray level) than regions of low atomic number/low mineral content (lower gray level). To date, qBEI has been widely used to study not only healthy human bone but also bone abnormalities obtained from clinical biopsies where both overt and subtle changes in mineralization were detected in these highly diverse bone tissue samples.[27]

The spatial resolution of qBEI is limited by the interaction volume between the primary electron beam and the specimen under analysis. According to the widely accepted protocol developed by Roschger and colleagues,[30] qBEI measurement is estimated to take into account a surface layer of a bone specimen that is ~0.5 to 1.5 μm in thickness, a value suggesting that any bone structural feature less than 0.5 μm (for example, small canaliculi or nanochannels) cannot be differentiated by this method. Stated in other words, such a value implies conceptually that qBEI becomes insensitive to changes in mineralization (mineral heterogeneity) at a scale <0.5 μm. These nanoscale alterations in mineral content have been studied recently through high-resolution imaging techniques, such as X-ray phase nanotomography[21] and FIB-SEM,[24] where significant changes in mineral content in the close vicinity (within a micrometer or so) of bone LCN boundaries have been reported. On the other hand, while the sensitivity of qBEI to scale has been calculated by Roschger and colleagues,[30] that level of spatial resolution remains hypothetical as just noted. Under this circumstance, the study here has also investigated whether and how a qBEI measurement might be impacted by the presence of nanochannels in human femoral cortical bone.

A recent work examining the contribution of the pericanalicular matrix to the mineral content in human cortical bone reported a positive correlation between LCN density and local calcium concentration in this tissue.[31] The calcium content increased with LCN density, an observation that contradicted the model in which bone matrix is viewed as a homogeneous mineralized material and traversed by only the LCN.[31] In this regard, the study suggested that the positive correlation observed was attributable to an active role of the LCN in mineral exchange with the surrounding pericanalicular matrix in which increased calcium content localized in the pericanalicular matrix overcompensated the porosity effect of the LCN.[31] In similar fashion to determine whether and how nanochannels may be associated with the mineral content in human cortical bone, the present work has quantified and correlated nanochannel volume with respect to local bone mineral content through FIB-SEM and qBEI data, respectively.

To examine the potential existence of nanochannels in human bone and investigate their putative role in mineralization as described above, healthy and undecalcified human femoral cortical bone was studied here by both FIB-SEM and qBEI to correlate the bone ultrastructure and bone calcium content. FIB-SEM in serial surface view mode was used to interrogate the bone subcanalicular structure with nanometer resolution in 3D and in tissue volumes exceeding tens of micrometers. By combining the FIB-SEM observations with qBEI measurements within the same tissue volume, subcanalicular nanochannels in human cortical bone were identified for the first time, and their porosities were found to have a significant impact on the calcium content of this tissue. These two parameters were determined to be inversely correlated, unlike their direct correlation reported in the LCN comprising human cortical bone.[31] The work presented here provides clear evidence of mineral heterogeneity at the nanometer scale of human cortical bone tissue and demonstrates importantly that qBEI measurements of bone calcium content should be based on a three-phase, rather than a two-phase, bone system that accounts for the presence of nanochannels in addition to collagen and hydroxyapatite. These data also suggest that the nanochannel network may be the remnant space between mineral ellipsoids during tissue mineralization in contrast to the LCN in its proposed role in facilitating and maintaining mineral homeostasis.

Materials and Methods

Specimen preparation

Human femoral cortical bone from autopsy samples (a few centimeters thick and wide) from the femoral midshaft of two male

donors (65 and 72 years old) without any known bone disease were investigated. The samples were obtained from the Unit of Forensic Gerontology, Center of Forensic Science and the Center for Anatomy and Cell Biology, Department of Anatomy at the Medical University of Vienna. This study was approved by the Ethics Commission of the Medical University of Vienna (EK no. 1757/2013).

All bone tissues were kept frozen at −20°C until specimen preparation. After thawing, the tissues were fixed in a formalin/ethanol (1:2) mixture for 72 hours, followed by dehydration in a graded ethanol series (80%, 96%, and 100%; 24 hours for each step except for 48 hours for 100% ethanol). The samples were next treated in a series of ethanol/acetone immersions: acetone/ethanol (1:1) for 24 hours, 100% acetone alone for 24 hours, acetone/ethanol (1:1) for 24 hours, and 100% ethanol alone for 48 hours. Finally, the samples were embedded in PMMA (Carl Roth GmbH + Co. KG, Karlsruhe, Germany) and trimmed with a water-cooled low-speed diamond saw (Buehler Isomet 1000, Buehler Ltd., Lake Bluff, IL, USA). The embedded samples were ground with a series of carbide grinding papers to expose the transverse sections of the human femoral cortical bone and then polished with a diamond suspension of 3 μm followed by 1 μm (Logitech PM5, Logitech Ltd., Glasgow, UK). To facilitate backscattered electron imaging, the polished samples were coated with carbon using an Agar carbon-coater (Agar Scientific Ltd., Essex, UK) to provide conducting surfaces during analyses.[30,32] Since the carbon thickness was variable from sample to sample, a carbon-coating correction was performed as described by Hartmann and colleagues[33] to minimize the coating effect on qBEI measurements.

Quantitative backscattered electron imaging

qBEI images were captured with a scanning electron microscope (SEM) equipped with a zirconium-coated Schottky field emission cathode (Zeiss SEM SUPRA 40; Carl Zeiss Microscopy, Oberkochen, Germany). The microscope was operated at 20 kV, the probe current was 300 ± 20 pA, and the working distance was 10 mm. Each image captured during measurement consisted of 1024 × 768 pixels with a pixel resolution of 1.76 μm/pixel for overview images or 0.5 μm/pixel for specific regions of interests (ROIs) as shown in Fig. 1*A*, *B*, for example. The image depth was 8-bit (gray level [GL] ranging from 0 to 255).

The principle of qBEI is that the backscattered electron yield is dependent on the (mean) local atomic number, Z, of the sample. For low values of Z, this relation is approximately linear. Thus, a calibration of the SEM with standards of known composition provides a quantitative relation between the measured GL and a local density of the sample. In the current study, before each measurement, the SEM signal was calibrated with carbon and aluminum standards of high purity.[33] Under the assumption that bone is a two-phase composite of collagen and varying fractions of stoichiometric hydroxyapatite (HA), a measured GL was related to a mineral density in wt% Ca[30] as

$$\mathrm{wt\%Ca} = 0.1733 \times \mathrm{GL} - 4.332. \quad (1)$$

It should be noted that the relation between wt% Ca and GL as shown above is valid only for a pixel resolution of 0.5 μm/pixel or lower because, under higher magnifications, in addition to the pure material contrast (Z-contrast), additional contrast may be present, resulting from different crystallographic orientations or orientation of bone lamellae, for example. In this instance, quantitative comparisons between wt% Ca and GL are strictly valid only for the same magnification settings of the instrument.

Focused ion beam-scanning electron microscopy

Ten ROIs without lacunae, canaliculi, or Haversian canals as observed under qBEI were further examined with FIB-SEM in serial surface imaging mode with a Zeiss crossbeam 540 (Carl Zeiss Microscopy). Carbon-coated specimens were oriented inside the FIB-SEM chamber so that the milling direction was approximately parallel to the bone lamellae and orthogonal to the major axis of the osteons comprising the samples (Fig. 1*C*, *D*). A coarse rectangular section was first milled with a 30 nA gallium beam at 30 kV acceleration voltage to provide a viewing channel for SEM observation (Fig. 1*C*, for example). The exposed surface of the rectangular section was fine-polished by lowering the ion beam current to 1.5 nA. Subsequently, the fine-polished block was serially milled by scanning the ion beam parallel to the surface of the cutting plane using an ion beam of 100 pA at 30 kV. After removal of each tissue slice, the freshly exposed surface was imaged at 1.6 kV acceleration voltage and 600 pA using both secondary electron (SE) and Inlens energy selective backscattered (EsB) detectors (EsB grid of 840–940 V). The slice thickness was roughly equivalent to the lateral resolution of 2D images, ranging from 5 to 7 nm (Fig. 1*E*). In a fully automated procedure, the milling was combined with SEM imaging in sequence (imaging, then sectioning and reimaging) to collect hundreds of serial images (Fig. 1*E*). Serial images were aligned (image registration) and then curtaining effects were reduced and background noise was removed with in-house python scripts in Anaconda (Anaconda Inc., Austin, TX, USA), following the procedure as described by Spehner and colleagues,[34] and Dragonfly (v 4.1; Object Research System Inc., Montreal, Canada). The resulting stacks of images were then segmented according to their structural features and the segmented structural components were visualized in 3D using surface rendering in Amira-Avizo (v 2020.1; Thermo Fisher Scientific and Zuse Institute, Berlin, Germany).

Analysis of the FIB-SEM images

To segment the nanochannels in 3D, a localized thresholding algorithm, Phansalkar,[35] was applied to the serial FIB-SEM images. The Phansalkar algorithm is known to allow separation of background and foreground, particularly in low-contrast grayscale images, and it is based on a combination of the local mean, local standard deviation, and parameters to constrain the calculation in certain conditions.[35] The segmented nanochannels were converted into stacks of binary images where the nanochannels appeared as black against a white background. These binary images were then processed in Dragonfly v 4.1 and an in-house python script in Anaconda (Anaconda Inc.) to filter out the extremely short/non-connected nanochannel segments that resulted from imaging background noise or the appearance of characteristic periodic banding from the collagen fibrils present in the samples. Finally, these images were superimposed over the original FIB-SEM images for manual inspection for the accuracy of nanochannel segmentation (Supplemental Movie S1).

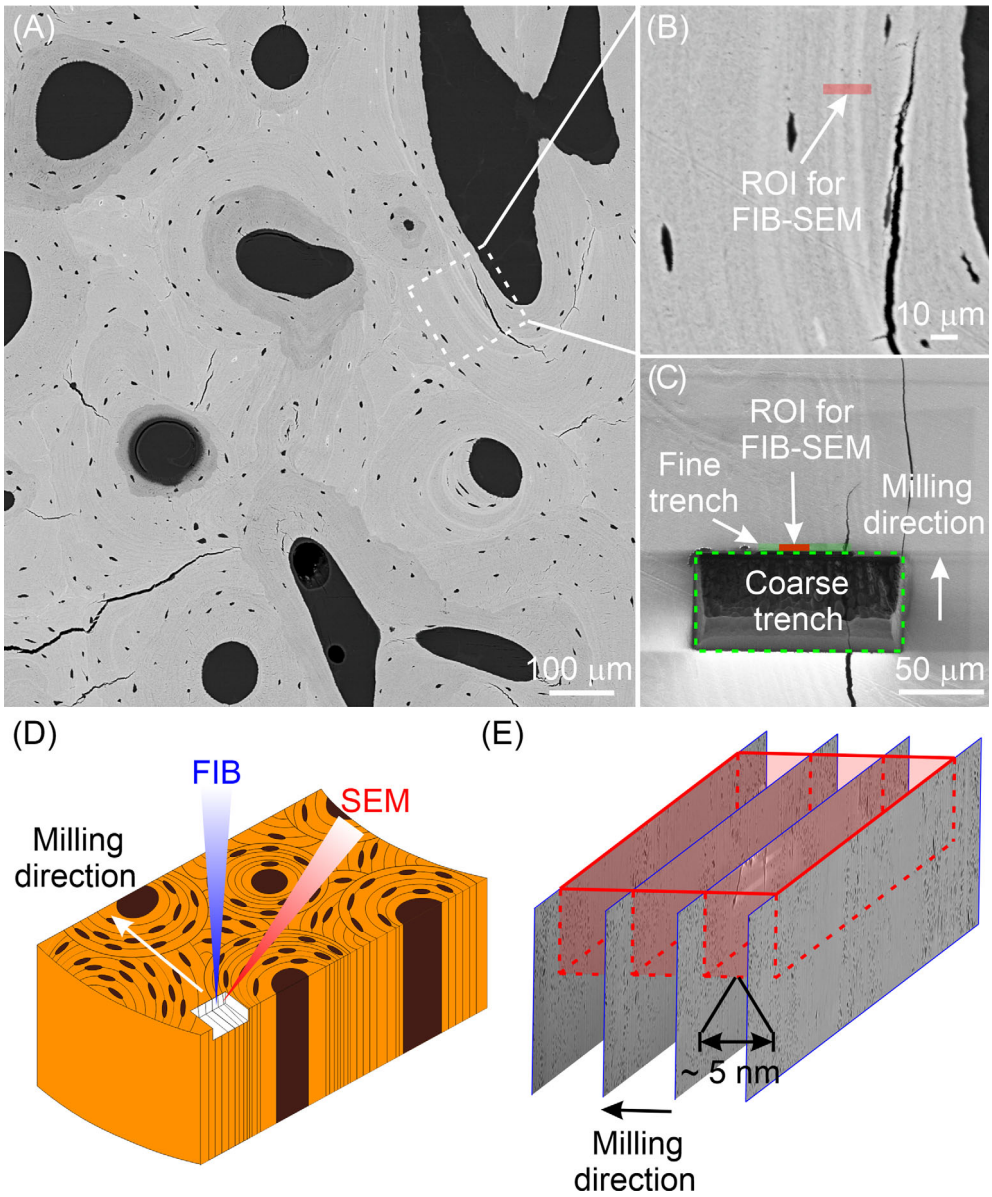

Fig. 1. Examination of human cortical bone using quantitative backscattered electron imaging (qBEI) and focused ion beam-scanning electron microscopy (FIB-SEM). (*A*) qBEI image of a representative tissue section obtained from the transverse plane of the femoral cortical bone of a 65-year-old male. Individual osteons comprise the tissue and are marked by a large central pore (black) representing the location of a Haversian canal, numbers of bone lamellae (light and dark gray), and small, dark pits that are osteocyte lacunae within the lamellae. The white-dashed rectangle denotes a region examined more closely with FIB-SEM. (*B*) The enlarged qBEI image corresponding to the white-dashed rectangle in (*A*). The red-shaded rectangle represents the region of interest (ROI) analyzed under FIB-SEM, and it traverses several layers of lamellae and cement lines associated with one or more osteons. There are a few osteocyte lacunae in the image, a microcrack and the periphery of a Haversian canal. (*C*) A SEM image of the sample surface showing a coarse trench milled by FIB (green-dashed rectangle) to reveal the ROI, which is then subjected to volume imaging under FIB-SEM. The red-shaded rectangle corresponds to the ROI in (*B*). A coarse trench is milled initially with a large ion beam current and a fine trench at the edge of the coarse trench is milled subsequently with a smaller current. The milling direction is indicated by an arrow in the figure. (*D*) A schematic diagram of the setup for FIB-SEM in serial surface imaging mode. The sample surface is positioned normal to the FIB (blue beam) and the milling direction is parallel to the bone lamellae and orthogonal to the major axis of the osteons. A milled trench is illustrated as a white region of the tissue. After each FIB milling, the newly revealed face of the trench is imaged by SEM (red beam), and this procedure of FIB milling followed by SEM imaging is performed in an iterative fashion to produce a stack of serial micrographs. (*E*) Illustration of serial images obtained by FIB-SEM. The red-dashed rectangles delineate the ROI in four imaging planes (blue frames) within the full ROI volume (red shading) for FIB-SEM analysis. The slice thickness between each serial image is ~5 nm.

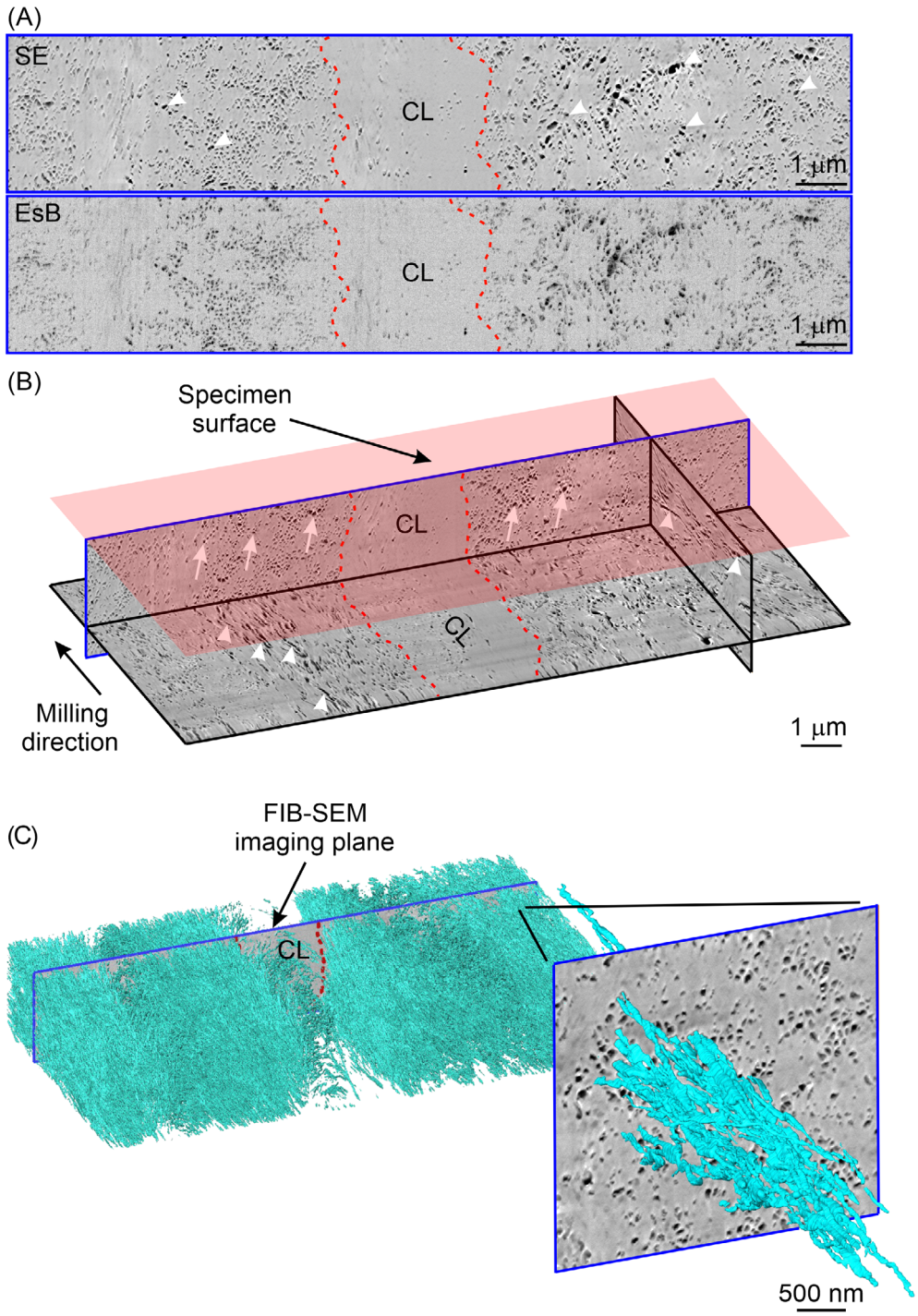

Fig. 2. Nanochannels in human femoral cortical bone revealed by focused ion beam-scanning electron microscopy (FIB-SEM). (*A*) Secondary electron (SE) and Inlens energy selective backscattered (EsB) images from a representative FIB-SEM volume showing the cement line (CL, red-dashed lines) and numerous dark pore-like features (arrowheads) in the lamellar bone. Notably, the CL has very few dark pore structures and there is no significant variation in the EsB gray level distribution across the CL and lamellar bone. The blue frames denote the imaging plane in FIB-SEM. (*B*) Perspective rendering of the three orthogonal planes of FIB-SEM imaging from the same volume of (*A*) and a reference plane (red/transparent specimen surface). Fine, dark pores are shown in the blue-framed imaging plane (white arrows). These pores correspond to the dark channel features in the other two orthogonal planes (white arrowheads). The CL (red-dashed lines) contains limited numbers of dark channels. (*C*) 3D surface rendering corresponding to (*A*) and (*B*) of the extracellular matrix network of bone intersecting with the FIB-SEM imaging plane (blue frame) in the background. Numerous nanochannels are shown in cyan and disposed at various angles to the imaging plane. The transverse profiles of these nanochannels are the dark pore features observed in (*A*) and (*B*). The cement line corresponding to the CL in (*A*) and (*B*) is outlined by red dashes. A small region of selected nanochannels from the 3D rendering of (*C*) intersecting with a portion of the FIB-SEM background image (blue frame) is enlarged and shows that the nanochannels are highly interconnected and predominantly oriented at a large angle to the FIB-SEM imaging plane.

Results

Morphology of nanochannels in human femoral cortical bone

FIB-SEM volume imaging with a 5 nm voxel size was used to examine human femoral cortical bone tissue volumes ($n = 10$; volume size range 61–138 μm^3; image width 15–30 μm; image height ~5–10 μm; depth ~3–8 μm) and revealed fine nanochannel structures penetrating the lamellar bone of all specimens (Fig. 2 and Supplemental Movie S2). These nanochannels appeared as dark pores when the imaging plane was perpendicular and across the layers of lamellae (Fig. 2*A*), and they were elongated in the form of narrow passages in the direction parallel to the lamellae in the other two orthogonal planes (Fig. 2*B*). The term, nanochannels, is used throughout this article to describe the nanochannel-like unmineralized spaces.

The nanochannels had an average diameter of ~30 nm, almost 10 times smaller than that of canaliculi reported in human bone.[11,21,36] The volume of the nanochannels within the lamellar bone varied from 6% to 13% for each of the 10 ROIs and averaged ~10% for all ROIs, a value five times higher than that of canaliculi found in human bone.[11,21,36] As shown in a representative 3D rendering of the nanochannels (Fig. 2*C* and Supplemental Movie S2), they interconnected to form a dense network where some individual nanochannels could be micrometers in length. By skeletonization of the segmented nanochannels using the scikit-image library,[37] the total cumulative length of nanochannels/unit volume of bone was estimated to range from 31 to 108 μm/μm^3 with an average value of 70 μm/μm^3. Assuming the total volume of bone in an average adult White skeleton is 1.75×10^{15} μm^3,[38] the total cumulative length of all nanochannels in the human skeleton may be calculated as ~1.23×10^8 km, three orders of magnitude longer than the reported values of human bone canaliculi.[36] On multiplying the total cumulative length of nanochannels by the cross-sectional perimeter of a nanochannel based on the diameter estimated above, the total surface area of the human nanochannel network is thus approximately 1.16×10^4 m^2, two orders of magnitude larger than the calculated value of human bone canaliculi.[36] A comparison between the derived parameters of the nanochannels and their reported measurements of the LCN in human bone is shown in Table 1.

Another notable observation is the number/unit area of the nanochannels and their distribution, which were found to be different in lamellar bone compared with the cement line (CL) of the specimens (Fig. 2). The CL had apparently fewer nanochannels/unit area compared with the same parameter analyzed in the neighboring lamellar bone (Fig. 2). Further, the backscattered electron imaging gray level of the fully mineralized regions (excluding the nanochannels) of the CL and lamellar bone did not show significant variation (Fig. 2*A*, EsB).

Relationship between nanochannel volume and calcium content

qBEI with a pixel size of 0.5 μm was performed on all 10 ROIs where FIB-SEM was conducted (Fig. 3*A*). To exclude the effects from porosities other than those of nanochannels, the tissue volumes from bone osteoid, Haversian canals, and lacunae, as well as canaliculi, were not considered in the analyses. A representative qBEI image is shown in Fig. 3*B*, where the red-shaded rectangle indicates the ROI. In this case, the ROI spanned two cement lines and multiple layers of lamellae with brighter backscattered signals (gray level) in the CL regions (white arrowheads) compared with the signals from lamellae. The calcium content (wt % Ca) for each pixel was calculated using eq. (1) (presented in Materials and Methods) based on the individual gray level intensity, and a plot profile of the ROI was subsequently obtained of average pixel intensity (*y* axis) versus distance across the ROI (*x* axis) (Fig. 3*B*, plot). It is clear that the cement lines are hypermineralized compared with the adjacent lamellar bone with a peak calcium content of ~28.2 wt% (Fig. 3*B*, plot), a value in agreement with that reported for older human bone.[40] After qBEI measurement, the volume corresponding to the ROI (red-shaded rectangle) was further analyzed using FIB-SEM, as demonstrated in Fig. 3*C*. To match the imaging resolution of qBEI (both spatial resolution and electron-sample interaction volume), the uppermost 500 nm layer of the acquired FIB-SEM volume was equally divided into smaller subvolumes, each with a width and depth of 500 nm (Fig. 3*C*). Within each subvolume, the nanochannels were segmented and their volume percentage (vol%) was subsequently calculated. As illustrated in the plot of Fig. 3*C*, the nanochannel volume (vol% nanochannels) varied between the subvolumes. Notably, there were far fewer nanochannels in the CL regions. Inverting the *y* axis of the vol% nanochannels plot provided a direct means of comparison between the changes in wt% Ca and vol% nanochannels across the ROI (Fig. 3*D*). In general, the wt% Ca has an inverse correlation with vol% of nanochannels. The dependency of wt% Ca on vol% nanochannels across all 10 ROIs may be found in Supplemental Fig. S1. The 10 ROIs (four from the 72-year-old male and six from the 65-year-old male) displayed a variability with no indications that inter-individual is larger than intra-individual variability. In a related context, each of the 10 ROIs also represents sampling from both osteonal and interstitial bone. In this instance, there is variability in wt% Ca between these two microstructural compartments as shown in (*D*) as one particular example in Fig. 3.

Fig. 4*A* represents each value of the wt% Ca obtained from qBEI measurements and the corresponding value of the vol% nanochannels found from FIB-SEM for every ROI analyzed in this study. Because the extracellular matrix of the CL is incompletely understood in terms of its composition, where it likely contains a considerable content of organic molecules in addition to type I collagen, the data points measured from the CL were excluded in Fig. 4*A*. Nonetheless, it is evident that the nanochannel volume is inversely correlated with the calcium content in the human femoral cortical bone—when the vol% nanochannels increases, the wt % Ca decreases (Fig. 4*A*). This inverse correlation was consistent across all 10 ROIs (Supplemental Fig. S2). As shown in Fig. 4*A*, there

Table 1. Comparison between Lacunocanalicular Network and Nanochannel Parameters in Human Bone[a]

Parameters	Lacunocanaliculi	Nanochannels
Diameter of a channel (nm)	360–380 [21,39]	30
Volume fraction	2.05% [36]	10%
Total volume (cm^3)	35.8 [36]	175
Length density (μm/μm^3)	0.074 [23]	70
Total cumulative length (km)	1.75×10^5 [36]	1.23×10^8
Total surface area (m^2)	2.15×10^2 [36]	1.16×10^4

[a]Note that the parameters of nanochannels are limited to human femoral cortical bone.

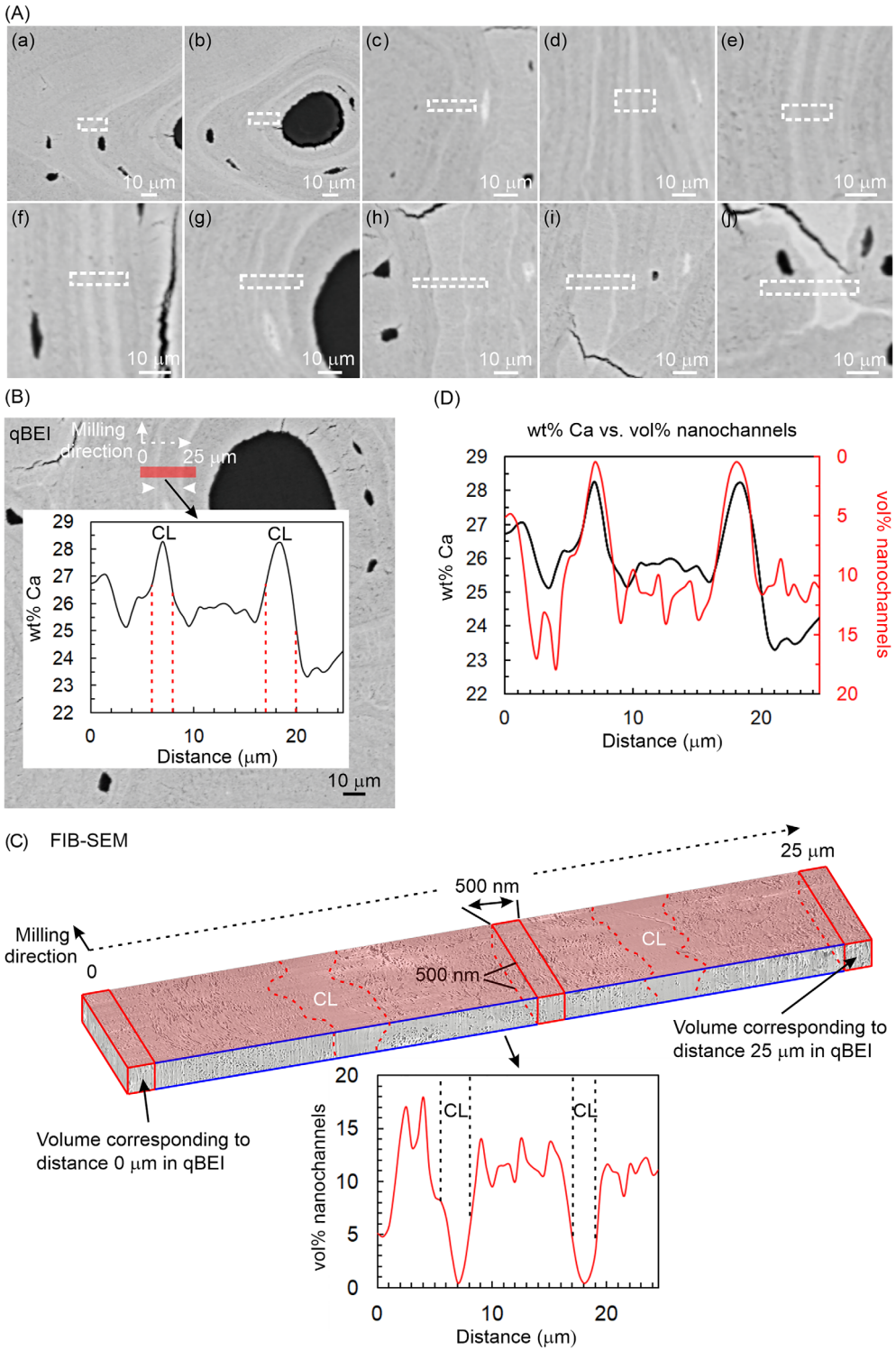

Fig. 3. Quantitative backscattered electron microscopy images from 10 different bone regions (*A*) and relationship between wt% Ca and vol% nanochannels in human femoral cortical bone (*B–D*). (*A*) The white-dashed rectangle in each panel indicates the region of interest (ROI) further analyzed with focused ion beam-scanning electron microscopy (FIB-SEM) imaging. (*a–d*) and (*e–j*) are ROIs from a 72-year-old male and a 65-year-old male femoral cortical bone specimen, respectively. Haversian canals, osteons, and other structural features evident in the panels are as defined in Fig. 1*A*. (*B*) A quantitative backscattered electron imaging (qBEI) image of a transverse section (*g*) from the femoral cortical bone of a 65-year-old male overlaid by a plot of the changes in wt% Ca across layers of lamellae and cement lines of the tissue. The red-shaded rectangle (25 μm in length, 5 μm in width) of the qBEI image represents the region for qBEI and FIB-SEM analyses. The narrow, irregular cement lines (arrowheads) can be identified by the higher gray value of the qBEI image. The plot shows that the wt% Ca varies from the left to right of the red-shaded rectangle (0–25 μm) with highest values overlapping the cement line (CL) regions. Red dashes

(Figure legend continues on next page.)

is also a significant scatter in the data plot, a result most likely attributable to the inherent heterogeneity of collagen fibril mineralization (that is, different degrees of mineralization of the fibrils, themselves). Additional measurements from the CL regions are shown in Supplemental Fig. S3 for reference.

Since the nanochannels may make a distinct contribution to the calcium content measurement with qBEI, bone at the material level is thus assumed to be comprised of three phases, type I collagen (Col), hydroxyapatite (HA), and nanochannels (NC). In other words: $V_{HA}+V_{Col}+V_{NC}=1$, where V_i represents the volume fraction of material i. Since the weight fraction of calcium in hydroxyapatite is 0.4, calculated from its chemical formula ($Ca_{10}(PO_4)_6OH_2$), the wt% Ca of a three-phase bone system is:

$$\mathrm{wt\%Ca}=\frac{0.4\,V_{HA}\,\rho_{HA}}{V_{HA}\,\rho_{HA}+V_{Col}\,\rho_{Col}+V_{NC}\,\rho_{NC}}=\frac{0.4\,k\,\rho_{HA}}{k\,\rho_{HA}+\rho_{Col}+V_{NC}\,(1+k)\rho_{NC}}, \quad (2)$$

where ρ_i denotes the mass density of material i, and k is the volume fraction ratio between hydroxyapatite and type I collagen ($k=V_{HA}/V_{Col}$). The known values for hydroxyapatite and collagen density are 3.18 and 1.4 g/cm^3, respectively.[41,42]

Based on this three-phase model of bone and that $V_{NC}\ll 1$, the measured wt% Ca can be correlated with vol% nanochannels through a linear equation:

$$\mathrm{wt\%Ca}\approx\frac{0.4\,k\,\rho_{HA}}{\rho_{Col}+k\,\rho_{HA}}\left(1-V_{NC}\frac{(1+k)\,\rho_{NC}}{\rho_{Col}+k\,\rho_{HA}}\right). \quad (3)$$

Here, the intercept of a line obtained from eq. (3) will determine the degree of mineralization of the collagen fibrils themselves as well as the volume fraction ratio between hydroxyapatite and collagen, k (V_{HA}/V_{Col}), and the slope of the line will determine the mass density of the nanochannels, ρ_{NC}. (For derivation of eq. (3), see Supplemental Material, Mathematical calculation.) For each of the 10 ROIs examined in this study, the linear eq. (3) was used to fit the paired values of wt% Ca and vol% nanochannels separately. The 10 different lines are presented in Supplemental Fig. S2, and their respective range of values of slopes and intercepts provides the calculated values of k (V_{HA}/V_{Col}) and ρ_{NC} as illustrated in Fig. 4*B*.

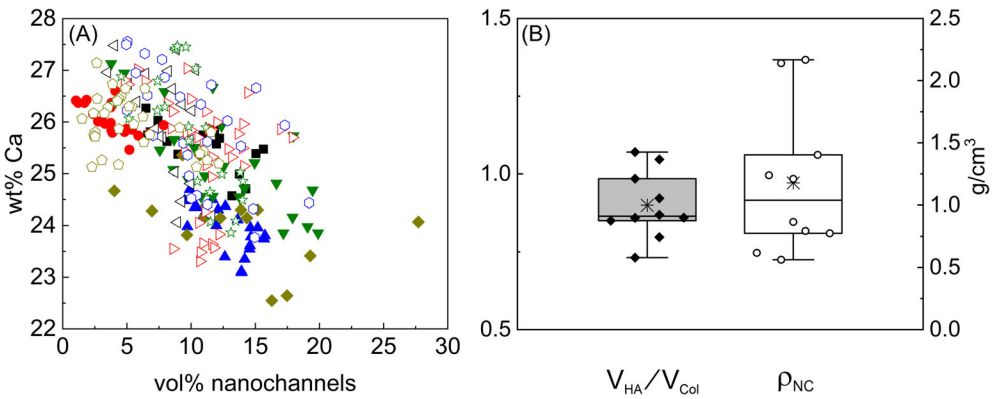

Fig. 4. Correlation between wt% Ca and vol% nanochannels in human femoral cortical bone. (*A*) Scatter plot of wt% Ca measured with quantitative backscattered electron imaging (qBEI) and the corresponding nanochannel volume obtained from focused ion beam-scanning electron microscopy (FIB-SEM) acquired from 10 different regions of interest (ROIs) excluding the cement line regions of the femoral bone. Different colors and shapes of the plotted points represent different ROI data sets. Overall, as the vol% nanochannels increases, wt% Ca decreases. (*B*) Box chart with individual data points of the volume fraction ratio between hydroxyapatite and collagen (V_{HA}/V_{Col}) and the mass density of nanochannel content (ρ_{NC}) based on the fitted values extracted from the correlation between wt% Ca and vol% nanochannels of (*A*). The boxes represent 50% of the data, limited by the upper and lower quartiles, with the median and mean indicated by a line and an asterisk, respectively, within each box. The whisker range is determined by the 5th and 95th percentiles of data. Each data point of the 10 ROIs (solid squares and open circles) overlapping the box plot represents each fitted value calculated from one ROI data set.

(Figure legend continued from previous page.)
demarcate the boundaries between the CL and lamellar bone. (*C*) 3D volume rendering of FIB-SEM from the red-shaded rectangle in (*B*) and the quantification of vol% nanochannels in the same tissue volume. The entire FIB-SEM volume is divided into subvolumes (red-outlined boxes) so that the width and depth of each subvolume (each 500 nm) matches the qBEI electron beam resolution. The irregular red dashes denote the boundaries of the CL and the blue lines indicate the FIB-SEM imaging plane. The vol% nanochannels is quantified for each subvolume, and the changes from the left to right of the entire tissue volume (0–25 μm) are plotted below the 3D rendering. The vol% nanochannels decreases in the CL regions (black dashes) compared with the rest of the analyzed volume of tissue. (*D*) Plot of changes in wt% Ca (black) measured by qBEI in (*B*) superimposed with vol% nanochannels (red) examined by FIB-SEM in (*C*). Note that the *y* axis scale of vol% nanochannels is inverted in this plot compared with the plot in (*C*). The two curves have similar shape, and their peak positions, locating the CL regions, are colocalized. When wt% Ca is maximum, vol% nanochannels is minimum.

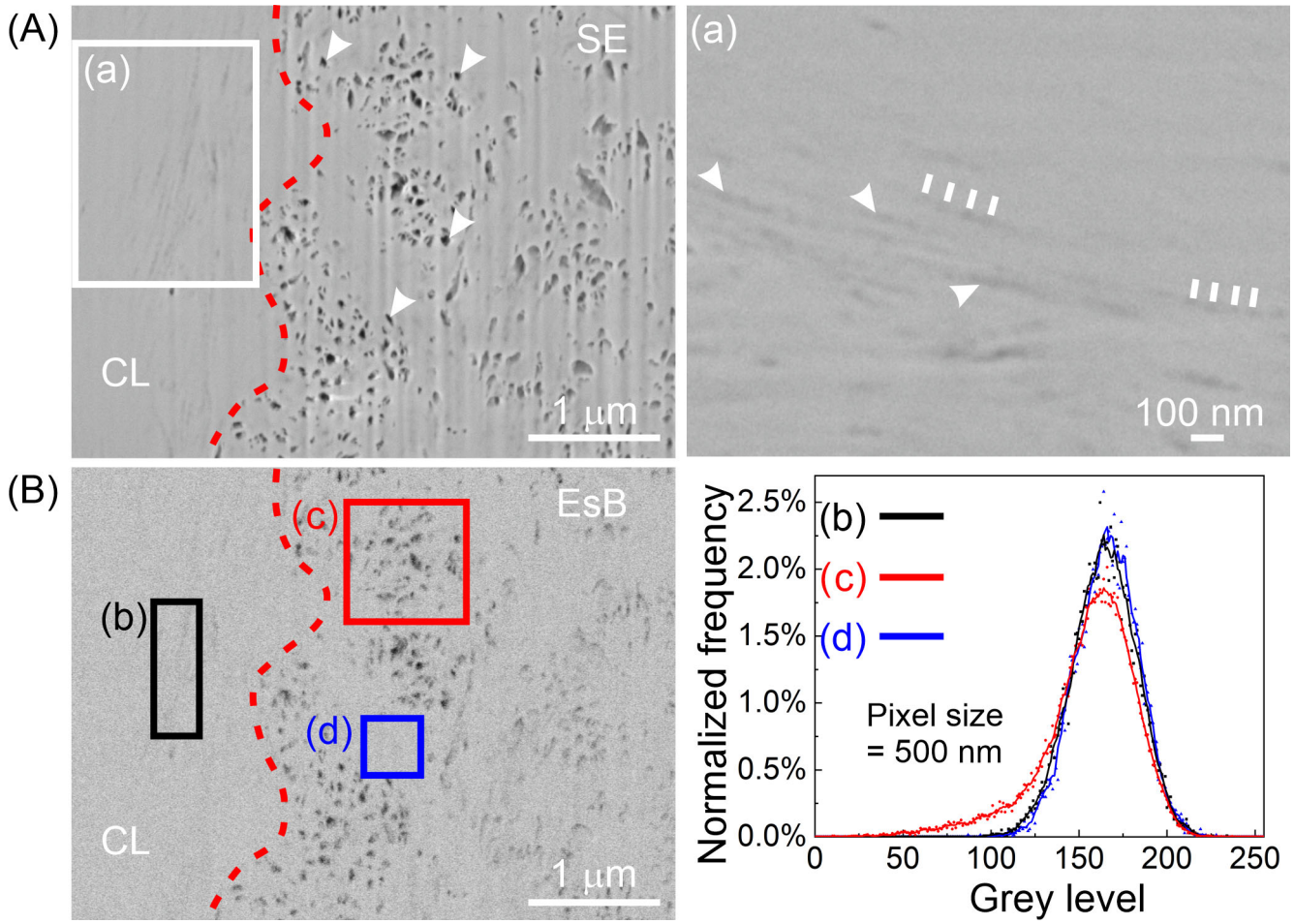

Fig. 5. Focused ion beam-scanning electron microscopy (FIB-SEM) images and gray level histograms of representative femoral cortical bone regions comprised in part of mineralized collagen fibrils and nanochannels. (*A*) A secondary electron (SE) image showing the cement line (CL, red-dashed line) to the left and numerous dark nanopores (arrowheads) within the lamellar bone aspect. A region of the CL (*a*) is enlarged and shown in the right panel, where multiple collagen fibrils can be observed (arrowheads) with their characteristic periodic D-banding pattern (~67 nm; white lines). (*B*) An energy selective backscattered (EsB) image from the same area of (*a*) showing a similar gray level in the CL and lamellar bone region. The black-enclosed area (*b*) in the CL is mainly comprised of partially and highly mineralized collagen fibrils, the red-enclosed area (*c*) in the lamellar bone is dominated by nanochannels, and the blue-enclosed area (*d*) in the lamellar bone consists principally of highly mineralized collagen fibrils. The lower right panel shows histograms of (*b*, *c*, and *d*) representing the frequency of gray level values normalized to the respective total enclosed black, red, and blue areas. The histograms were drawn based on an image resolution of 500 nm/pixel. The fitted peak positions from the three areas closely colocalize. The peak position of (*d*) is shifted slightly to higher gray values and is of greater frequency compared with the peak positions of (*b*) and (*c*). The curve (*c*) has greater frequency of gray values in the ~50–140 range and the peak (*c*) is of lower frequency compared with the curves and peaks of (*b*) and (*d*).

From these data, the degree of mineralization of the collagen fibrils was estimated to be 26.8 ± 1.0 wt% Ca (Supplemental Fig. S2) and the volume fraction ratio between hydroxyapatite and collagen was ~0.9 ± 0.1 across the 10 ROIs, whereas the mass density of nanochannels ranged from 0.6 to 2.1 g/cm^3 with a median value of 1.0 g/cm^3 (Fig. 4*B*). This nanochannel density range encompasses the density of collagen as well as the density of PMMA, the embedment resin for the specimens, which is reported to be approximately 1.18 g/cm^3.[43]

Since the nanochannels appeared throughout the bone tissue in an inhomogeneous manner, as mentioned above, it was not uncommon to observe areas largely occupied by partially mineralized collagen fibrils with apparent D-banding, whereas nanochannels were completely absent from the same regions (for instance, Fig. 5*A*). One example, representative of similar ROIs, is shown in Fig. 5, and the comparison of gray level histograms (direct indicators for wt% Ca distribution) of nanochannel absent areas (Fig. 5*Bb*) to those from other areas that were predominantly occupied by nanochannels (Fig. 5*Bc*) showed a similar peak position of the gray level (the most frequently appearing gray level representing wt% Ca) with only slight differences in the shape of the curves (Fig. 5*B*, plot). More specifically, the area principally comprised by nanochannels was shifted to lower mineralization with broadening of the curve (Fig. 5*B*, plot). Because areas such as that shown in Fig. 5*Bb* may be found within the CL and may contain organic building blocks other than the known collagen, additional areas in the bone tissue without apparent nanochannels or partially mineralized collagen fibrils

were also chosen for analysis (Fig. 5*Bd*). However, the gray level histograms from these areas (such as Fig. 5*Bd*) were not translated into bone mineralization density distribution (BMDD) curves because the EsB signals obtained under FIB-SEM could not be calibrated using the same method as described by Roschger and colleagues.[30] It should also be noted that the pixel resolution to evaluate these gray scale histograms was 500 nm, and therefore much smaller than that typically used in the standard BMDD of clinical biopsies,[27] where the size of one pixel is in the micrometer range and thus larger than the entire area of interest of (*b*), (*c*), and (*d*) in Fig. 5. Nonetheless, the summary histogram data obtained (Fig. 5*B*, plot) demonstrated that similar wt % Ca measures from different regions of the bone tissue may be accounted for by contributions from entirely different structural features, including in particular their constituent nanochannels as well as partially mineralized collagen fibrils.

Discussion

3D FIB-SEM volume imaging of undecalcified human femoral cortical bone has revealed a previously unreported nanochannel system much more extensive than the well known LCN. On excluding the LCN in the tissue volume measured by qBEI, the calcium content (wt% Ca) of human femoral cortical bone was found to be systematically dependent on the volume fraction of nanochannels (vol% nanochannels), and this result suggests therefore a revised understanding of the current interpretation of qBEI data. More importantly, the inverse correlation between wt% Ca and vol% nanochannels indicates an "inert" role of nanochannels in mineral exchange as opposed to the "active" role of the LCN, where the nanochannels are suggested to provide additional pathways for mineral ion and small molecule transport throughout bone matrix without accumulating mineral in the vicinity of perinanochannel zones.

Interconnected nanochannel structures with similar diameters (~30 to 50 nm) have been reported recently in mineralizing turkey leg tendon[15] and at the mouse bone-cartilage interface.[17] The size/diameter of these nanochannels, though discovered in different species and types of mineralized tissues, is one order of magnitude smaller than that of human bone canaliculi.[36,44] The organization of the nanochannels in the tissue volumes examined in the present study appeared to be anisotropic and highly directional where a single nanochannel could be micrometers long before intersecting with another nanochannel (Fig. 2). This observation is in line with the reported data from turkey leg tendon, where the nanochannels are unidirectional and parallel to each other as well as to the collagen fibrils comprising this tissue.[15] The finding is also consistent with results from the mouse bone-cartilage interface, where the nanochannels are in principle aligned with the CL plane.[17] One interesting feature of the nanochannels is their heterogeneous appearance in the mineralized tissue matrix, where the cement lines contained far fewer nanochannels compared with the lamellar bone (Figs. 2 and 3). Such heterogeneity was also found in the study of the mouse bone-cartilage interface, although the cement lines were reportedly devoid of any nanochannels.[17] This difference is perhaps attributable to variations in organic components of the cement lines in mouse and human bones. Concerning the volume fraction of the nanochannels or nanochannel volume, human cortical bone, on average, contained more nanochannels in a fixed tissue volume compared with that in mouse bone (~10% versus 4%).[17] Despite these morphological differences between the nanochannels found in such varying biological systems (human bone, turkey leg tendon, the mouse bone-cartilage interface), their several shared common features of small nanochannel size, the extent to which the nanochannel network penetrates the extracellular matrix (vol% nanochannels), and the anisotropic arrangement of the nanochannel network (directionality) imply a ubiquitous nature of the nanochannels in biomineralized tissues.

The presence of these fine nanochannels has significant impact on the qBEI measurement. Numerous studies have used qBEI to characterize the mineralization heterogeneity in human bone at a microscopic scale.[27,45] Such variation in mineral concentration is also evident in the present study, where the calcium content (wt% Ca) ranges from 23% to 27% within one ROI, when the CL is excluded from consideration (Fig. 3), and from 22% to 28% across the 10 ROIs analyzed here (Fig. 4*A*). However, the imaging resolution of qBEI is limited in distinguishing mineralization heterogeneity at the nanometer scale. In this regard, an example in the current study is represented by the CL, the tissue component of the human cortical bone separating newer osteons from older interstitial bone (Fig. 3). Although the precise material composition of the CL is still incompletely understood,[46,47] there is a general agreement that the CL contains a higher mineral content compared with that of lamellar bone, a conclusion supported by previous qBEI, energy-dispersive X-ray spectroscopy, and X-ray fluorescence tomography work,[40,48,49] and also confirmed in the present qBEI study demonstrating hypermineralization of the CL in human femoral cortical bone (Fig. 3). However, within the same volume measured here by qBEI, it is interesting to note that the gray level of individual pixels obtained using EsB during FIB-SEM imaging appears to be similar to that from the lamellar bone (Figs. 2 and 5; Supplemental Fig. S4). The only noticeable difference between the cement lines and lamellar bone is their different levels of nanochannel volume. Therefore, a possible explanation for the measured hypermineralized state of cement lines may be their fewer constituent nanochannels (yielding lower nanochannel volume) rather than the degree of mineralization of the organic matrix.

The influence of nanochannel volume on measured calcium content is also clearly demonstrated in lamellar bone regions (Figs. 3 and 4*A*), where wt% Ca is largely dependent on vol% nanochannels. This observation suggests that the interpretation of a qBEI measurement is far more complex than what was previously considered. Conventionally, the conversion from backscattered gray level to calcium content using qBEI is dependent on the assumption that bone is a two-phase material comprised of collagen and hydroxyapatite. The current study, however, clearly demonstrates that qBEI is determined by not only the presence and content of collagen and mineral but also the inclusion of the nanochannel network. Thus, there is a need to think of bone as at least a three-phase material, consisting of collagen, hydroxyapatite, and nanochannels, when interpreting qBEI results. Based on the "three-phase" system, a linear equation has been developed to correlate wt% Ca and vol% nanochannels, leading to the extrapolation of the degree of mineralization associated with collagen fibrils excluding the nanochannels and the volume fraction ratio between hydroxyapatite and collagen (V_{HA}/V_{Col}). The derived hydroxyapatite/collagen volume fraction ratio has a narrow range (Fig. 4*B*) and is consistent with reported literature values,[50] whereas the values of wt% Ca of the collagen fibrils are significantly higher than the reported values in human bone based on standardized

evaluation of qBEI.[27] The conventional interpretation of a qBEI measurement thus underestimates the "true" degree of mineralization of the organic matrix.

A linear correlation between calcium content and nanochannel volume was found across the 10 ROIs analyzed in this study (Fig. 4*A* and Supplemental Fig. S2). In contrast to the positive correlation found between the local calcium concentration and LCN volume in bone as shown in the work by Roschger and colleagues,[31] the inverse correlation found between calcium content and nanochannel volume in the present study implies an "inert" network where matrix mineralization is independent of the nanochannels. More specifically, the nanochannels simply represent the extracellular matrix devoid of mineralized collagen, and consequently the qBEI signal would vary according to the density of the nanochannel network. In contrast to the suggested "active" role of the LCN in mineral exchange, where elevated levels of calcium were found in the vicinity of the canaliculi and thus provided immediate mineral access to osteocytes,[31] the nanochannels do not appear to accumulate calcium in the perinanochannel zones. This concept of an "inert" nanochannel network is consistent with the recent proposal that nanochannels form during tissue maturation as the remnants of the peripheral spaces between progressively growing mineral ellipsoids.[17] These ellipsoidal mineral structures, which have also been termed as "tesselles,"[51-53] have been recently described and systematically reviewed in a variety of biomineralized tissues.[51,53,54] A point may be raised as to whether nanochannels remain a persistent feature of bone throughout its life or whether they may be reduced or eliminated as matrix mineralization progresses. The data here present no immediate evidence to address this question. However, the observation in this study that "older bone" typically maintains a higher calcium content suggests that such bone is generally associated with decreased nanochannel volume. Speculatively, then, nanochannel volume decreases with the progression of mineralization. Because all the measured volumes, including those of interstitial bone but with the exception of the cement line, in the present investigation were found to contain nanochannels, it appears unlikely that the nanochannels are completely eliminated in the mature bone tissues.

The potential role of the nanochannels in mineralization was further elaborated through a calculated mass density of nanochannel content. Despite data scattered over a wide range, it was shown that the nanochannels could accommodate PMMA, the embedment resin for the bone specimen, as a possible infiltrating constituent (Fig. 4*B*). This measurement suggests that there is a possibility that the nanochannels are spaces between mineralized collagen fibrils that could provide pathways for ion and mineral precursor transport. Based on calculation of ρ_{NC}, the possibility cannot be excluded that nanochannels may be comprised of various organic molecules rather than being only empty and passive extracellular space. In this instance, more rigorous chemical analysis will be required to identify definitive nanochannel composition. In the absence of such information nonetheless, the collective data found in this study have provided evidence for the presence of nanochannels. A plausible conception is that nanochannels could provide pathways complementary to those of the LCN in conducting ions and small molecules to the bone extracellular matrix. In this proposed consideration, the nanochannels assist in transport of those ions and small molecules to the farthest reaches of the matrix that are inaccessible to the LCN network because of its size constraints. Being much smaller than the LCN pathways, the nanochannels have the capacity to penetrate the matrix to greater distances and extent, delivering the ions and small molecules to their target, the nascent and growing mineral ellipsoids. Thus, conceptually, there would be transport of solutes through the nanochannel network as a means of maintaining and sustaining mineral homeostasis of bone. Definitive evidence that might document these speculative features of the nanochannels is not yet forthcoming.

Given the possible role of the nanochannels in ion and small molecule transport throughout the skeleton and the astonishing comparison in certain basic physical parameters of the nanochannels to the LCN of human bone (Table 1), it is valuable to consider the nanochannel system for simulation in the context of mechanotransduction.[5,55] Many studies have shown that the morphology and connectivity of the LCN influence the liquid mass transport and flow velocities inside the LCN and thus significantly impact cellular physiology.[56,57] The nanochannels could, in a similar or complementary manner to that of the LCN, increase the extent and efficiency of distribution and transportation of ions and small molecules throughout the mineralizing tissue. To date, however, virtually all simulations of permeability of human bone porosities have been limited to vascular and LCN pores.[22,44,58,59] The discovery of a subcanalicular network in bone reported in the present study is an additional factor in this context. It should be noted that nanoscale porosity that gives rise to bone poroelasticity and interstitial fluid permeability has been noted in the published literature.[44] Such porosity in bone, characterized by small spaces of various sizes that are disconnected and isolated in the bone matrix, is quite different and not to be confused with the nanochannels, which are found and described here as interconnected conduit-like structures forming an extensive network throughout the bone matrix and complementary to the LCN. Considering the fine size, the substantial surface area and the complexity of the network of nanochannels described here, a comprehensive simulation model that incorporates porosities across several length scales (for example, Haversian canals, the LCN, and nanochannels) would be extremely challenging to develop, yet it could potentially shed new light at an unprecedented structural level on the critical character of ion and small molecule transport in human bone.

This study involved a limited number of human donor specimens, few analyzed samples, and only selected ROIs, which were restricted for investigation principally because of the time-consuming approach of imaging by means of 3D FIB-SEM. Despite these shortcomings, the summary results of the present work were consistent across all tissue volumes that were examined, and the collected data showed a clear correlation between the calcium content and nanochannel volume of the samples. That being said, future studies including larger and more diverse sample groups of different sex, age, and anatomical location should be conducted to verify the findings reported here. Additionally, osteoid and poorly mineralized regions (below 17.5 wt % Ca) were not included in the current study because of the inherent nature of the samples (old age) and the technical restrictions of qBEI.[60] Therefore, the outcome of this study does not necessarily extrapolate to newly mineralized regions and/or the mineralization front of femoral cortical bone specimens. A further concern was considerable scattering of the data points in the correlation plots between calcium content and nanochannel volume, a result which led to a wide range of values in the estimated mass density of nanochannels. This scattering could be attributed to variations in the degree of mineralization of the collagen fibrils themselves as well as uncertainty in the

electron interaction volume with the specimen under qBEI. However, the inverse correlation between the calcium content and nanochannel volume persists even when the evaluation of nanochannel volume was adjusted from a tissue volume depth of 500 nm to 1 μm (data not shown). Finally, questions may arise about potential artifacts that may be caused by either sample preparation or the FIB-SEM imaging technique itself. Considering that the nanochannel morphologies presented in this study are comparable to those obtained in the earlier turkey leg tendon study,[15] in which the tissue was prepared by both traditional chemical fixation and high-pressure freezing followed by freeze substitution, it is unlikely that the human bone nanochannels found here were induced by the methodologies of the current study. In addition, the lack of nanochannels in the cement line supports the notion that the nanochannels are true biological and not artifactual structural features.

In conclusion, an interconnected nanochannel network found in human femoral cortical bone was shown to be correlated with the calcium content measured by qBEI. Based on this correlation, it was suggested that bone material be reconsidered as a three-phase system, mainly comprised of collagen, mineral (hydroxyapatite), and nanochannels, when estimates of its local calcium content are made based on gray level measurements from backscattered electron imaging. The work presented here also highlights the heterogeneity in bone tissue mineralization at the nanometer scale. Finally, the data have implications for understanding the means by which mineral ions and/or mineral precursors may be transported through the extracellular milieu. In this instance, the nanochannels may provide conduits and pathways complementary to those of the LCN. Additional studies of human bone to elaborate the precise chemical composition within the nanochannels, the formation and development of the nanochannels, and the mineral propagation putatively associated with the nanochannels will describe more completely the exact role of nanochannels in the onset and progression of bone mineralization.

Conflicts of Interest

The authors declare no competing interests.

Acknowledgments

The authors are grateful to Sonja Lueger and Petra Keplinger and Phaedra Messmer (Ludwig Boltzmann Institute of Osteology, Vienna, Austria) for sample preparation, polishing, and qBEI imaging. The authors also thank Hubert Taieb, PhD, for the MATLAB code for dividing the FIB-SEM imaging volume into equal subvolumes; Clemens Schmitt, PhD, for technical support with FIB-SEM imaging; and Heike Runge for sample coating (all members of the Department of Biomaterials at the Max Planck Institute of Colloids and Interfaces). SB and MAH gratefully acknowledge financial support from the AUVA (research funds of the Austrian workers compensation board) and OEGK (Austrian Social Health Insurance Fund). PF and RW acknowledge support from the Max Planck Queensland Centre for the Materials Science of Extracellular Matrices. Open Access funding enabled and organized by Projekt DEAL.

Author Contributions

Tengteng Tang: Conceptualization; data curation; formal analysis; investigation; methodology; validation; visualization; writing – original draft; writing – review and editing. **William Landis:** Formal analysis; investigation; validation; writing – review and editing. **Stéphane Blouin:** Data curation; formal analysis; investigation; methodology; validation; writing – review and editing. **Luca Bertinetti:** Conceptualization; formal analysis; investigation; methodology; validation; writing – review and editing. **Markus A. Hartmann:** Data curation; formal analysis; investigation; methodology; validation; writing – review and editing. **Andrea Berzlanovich:** Resources; writing – review and editing. **Richard Weinkamer:** Formal analysis; investigation; validation; writing – review and editing. **Wolfgang Wagermaier:** Conceptualization; formal analysis; funding acquisition; investigation; methodology; project administration; resources; supervision; validation; writing – review and editing. **Peter Fratzl:** Conceptualization; formal analysis; funding acquisition; investigation; methodology; project administration; resources; supervision; validation; writing – review and editing.

Peer Review

The peer review history for this article is available at https://publons.com/publon/10.1002/jbmr.4753.

References

1. Weiner S, Wagner HD. The material bone: structure-mechanical function relations. Annu Rev Mater Sci. 1998;28(1):271-298.
2. Reznikov N, Shahar R, Weiner S. Bone hierarchical structure in three dimensions. Acta Biomater. 2014;10(9):3815-3826.
3. Fratzl P, Weinkamer R. Nature's hierarchical materials. Prog Mater Sci. 2007;52(8):1263-1334.
4. Currey JD. Bones. Princeton, NJ: Princeton University Press; 2002.
5. Fritton SP, Weinbaum S. Fluid and solute transport in bone: flow-induced mechanotransduction. Annu Rev Fluid Mech. 2009;41(1):347-374.
6. Boskey AL. In Nordin BEC, ed. Calcified tissues: chemistry and biochemistry. London: Springer; 1988 pp 171-186.
7. Choi JUA, Kijas AW, Lauko J, Rowan AE. The mechanosensory role of osteocytes and implications for bone health and disease states. Front Cell Dev Biol. 2022;9:1-23.
8. Robling AG, Bonewald LF. The osteocyte: new insights. Annu Rev Physiol. 2020;82:485-506.
9. Qing H, Bonewald LF. Osteocyte remodeling of the perilacunar and pericanalicular matrix. Int J Oral Sci. 2009;1(2):59-65.
10. Wang L. Solute transport in the bone lacunar-canalicular system (LCS). Curr Osteoporos Rep. 2018;16(1):32-41.
11. Schneider P, Meier M, Wepf R, Müller R. Towards quantitative 3D imaging of the osteocyte lacuno-canalicular network. Bone. 2010;47(5):848-858.
12. Goggin PM, Zygalakis KC, Oreffo RO, Schneider P. High-resolution 3D imaging of osteocytes and computational modelling in mechanobiology: insights on bone development, ageing, health and disease. Eur Cell Mater. 2016;31:264-295.
13. Wittig NK, Laugesen M, Birkbak ME, et al. Canalicular junctions in the osteocyte lacuno-canalicular network of cortical bone. ACS Nano. 2019;13(6):6421-6430.
14. Kerschnitzki M, Kollmannsberger P, Burghammer M, et al. Architecture of the osteocyte network correlates with bone material quality. J Bone Miner Res. 2013;28(8):1837-1845.
15. Zou Z, Tang T, Macías-Sánchez E, et al. Three-dimensional structural interrelations between cells, extracellular matrix, and mineral in normally mineralizing avian leg tendon. Proc Natl Acad Sci. 2020;117(25):14102-14109.
16. Macías-Sánchez E, Tarakina NV, Ivanov D, Blouin S, Berzlanovich AM, Fratzl P. Spherulitic crystal growth drives mineral deposition patterns in collagen-based materials. Adv Funct Mater. 2022;32(31):2200504.

17. Tang T, Landis W, Raguin E, et al. A 3D network of nanochannels for possible ion and molecule transit in mineralizing bone and cartilage. Adv Nano Biomed Res. 2022;2(8):2100162.
18. Varga P, Pacureanu A, Langer M, et al. Investigation of the three-dimensional orientation of mineralized collagen fibrils in human lamellar bone using synchrotron X-ray phase nano-tomography. Acta Biomater. 2013;9(9):8118-8127.
19. Raguin E, Rechav K, Shahar R, Weiner S. Focused ion beam-SEM 3D analysis of mineralized osteonal bone: lamellae and cement sheath structures. Acta Biomater. 2021;121:497-513.
20. Teti A, Zallone A. Do osteocytes contribute to bone mineral homeostasis? Osteocytic osteolysis revisited. Bone. 2009;44(1):11-16.
21. Hesse B, Varga P, Langer M, et al. Canalicular network morphology is the major determinant of the spatial distribution of mass density in human bone tissue: evidence by means of synchrotron radiation phase-contrast nano-CT. J Bone Miner Res. 2015;30(2):346-356.
22. Bortel E, Grover LM, Eisenstein N, et al. Interconnectivity explains high canalicular network robustness between neighboring osteocyte lacunae in human bone. Adv NanoBiomed Res. 2022;2(4):2100090.
23. Repp F, Kollmannsberger P, Roschger A, et al. Spatial heterogeneity in the canalicular density of the osteocyte network in human osteons. Bone Rep. 2017;6:101-108.
24. Ayoubi M, Tol AF, Weinkamer R, et al. 3D interrelationship between osteocyte network and forming mineral during human bone remodeling. Adv Healthc Mater. 2021;10(12):2100113.
25. Fratzl P, Gupta HS, Paschalis EP, Roschger P. Structure and mechanical quality of the collagen–mineral nano-composite in bone. J Mater Chem. 2004;14(14):2115-2123.
26. Gupta HS, Stachewicz U, Wagermaier W, Roschger P, Wagner HD, Fratzl P. Mechanical modulation at the lamellar level in osteonal bone. J Mater Res. 2006;21(8):1913-1921.
27. Roschger P, Paschalis EP, Fratzl P, Klaushofer K. Bone mineralization density distribution in health and disease. Bone. 2008;42(3):456-466.
28. Ruffoni D, Fratzl P, Roschger P, Klaushofer K, Weinkamer R. The bone mineralization density distribution as a fingerprint of the mineralization process. Bone. 2007;40(5):1308-1319.
29. Boyde A, Jones SJ, Aerssens J, Dequeker J. Mineral density quantitation of the human cortical iliac crest by backscattered electron image analysis: variations with age, sex, and degree of osteoarthritis. Bone. 1995;16(6):619-627.
30. Roschger P, Fratzl P, Eschberger J, Klaushofer K. Validation of quantitative backscattered electron imaging for the measurement of mineral density distribution in human bone biopsies. Bone. 1998;23(4):319-326.
31. Roschger A, Roschger P, Wagermaier W, et al. The contribution of the pericanalicular matrix to mineral content in human osteonal bone. Bone. 2019;123:76-85.
32. Roschger P, Gupta HS, Berzlanovich A, et al. Constant mineralization density distribution in cancellous human bone. Bone. 2003;32(3):316-323.
33. Hartmann MA, Blouin S, Misof BM, et al. Quantitative backscattered electron imaging of bone using a thermionic or a field emission electron source. Calcif Tissue Int. 2021;109(2):190-202.
34. Spehner D, Steyer AM, Bertinetti L, et al. Cryo-FIB-SEM as a promising tool for localizing proteins in 3D. J Struct Biol. 2020;211(1):107528.
35. Phansalkar N, More S, Sabale A, Joshi M. Adaptive local thresholding for detection of nuclei in diversity stained cytology images. 2011 International Conference on Communications and Signal Processing, Kerala, India: IEEE; 2011. p. 218–20.
36. Buenzli PR, Sims NA. Quantifying the osteocyte network in the human skeleton. Bone. 2015;75:144-150.
37. van der Walt S, Schönberger JL, Nunez-Iglesias J, et al. Scikit-image: image processing in python. PeerJ. 2014;2:e453.
38. Parfitt AM. The physiologic and clinical significance of bone histomorphometric data. In Recker RR, ed. Bone histomorphometry: techniques and interpretation. Boca Raton, FL: CRC Press; 1983 pp 143-223.
39. Varga P, Hesse B, Langer M, et al. Synchrotron X-ray phase nano-tomography-based analysis of the lacunar–canalicular network morphology and its relation to the strains experienced by osteocytes in situ as predicted by case-specific finite element analysis. Biomech Model Mechanobiol. 2015;14(2):267-282.
40. Milovanovic P, vom Scheidt A, Mletzko K, et al. Bone tissue aging affects mineralization of cement lines. Bone. 2018;110:187-193.
41. Ghedjemis A, Ayeche R, Benouadah A. A comparative study on physicochemical properties of hydroxyapatite powder prepared from bovine and dromedary bone. J Aust Ceram Soc. 2022;58(2):607-616.
42. Lees S, Heeley JD. Density of a sample bovine cortical bone matrix and its solid constituent in various media. Calcif Tissue Int. 1981;33(1):499-504.
43. Chung JP, Seong YM, Kim TY, et al. Development of a PMMA phantom as a practical alternative for quality control of gamma knife® dosimetry. Radiat Oncol. 2018;13(1):1-9.
44. Cardoso L, Fritton SP, Gailani G, Benalla M, Cowin SC. Advances in assessment of bone porosity, permeability and interstitial fluid flow. J Biomech. 2013;46(2):253-265.
45. Stockhausen KE, Qwamizadeh M, Wölfel EM, et al. Collagen fiber orientation is coupled with specific nano-compositional patterns in dark and bright osteons modulating their biomechanical properties. ACS Nano. 2021;15(1):455-467.
46. McKee MD, Nanci A. Osteopontin at mineralized tissue interfaces in bone, teeth, and osseointegrated implants: ultrastructural distribution and implications for mineralized tissue formation, turnover, and repair. Microsc Res Tech. 1996;33(2):141-164.
47. McKee MD, Nanci A. Osteopontin and the bone remodeling sequence. Ann N Y Acad Sci. 1995;760:177-189.
48. Skedros JG, Holmes JL, Vajda EG, Bloebaum RD. Cement lines of secondary osteons in human bone are not mineral-deficient: new data in a historical perspective. Anat Rec Part A Discov Mol Cell Evol Biol. 2005;286A(1):781-803.
49. Wittig NK, Palle J, Østergaard M, et al. Bone biomineral properties vary across human osteonal bone. ACS Nano. 2019;13(11):12949-12956.
50. Currey JD. The design of mineralised hard tissues for their mechanical functions. J Exp Biol. 1999;202(23):3285-3294.
51. McKee MD, Buss DJ, Reznikov N. Mineral tessellation in bone and the stenciling principle for extracellular matrix mineralization. J Struct Biol. 2022;214(1):107823.
52. Buss DJ, Reznikov N, McKee MD. Crossfibrillar mineral tessellation in normal and Hyp mouse bone as revealed by 3D FIB-SEM microscopy. J Struct Biol. 2020;212(2):107603.
53. Buss DJ, Kröger R, McKee MD, Reznikov N. Hierarchical organization of bone in three dimensions: a twist of twists. J Struct Biol X. 2022;6:100057.
54. Micheletti C, Hurley A, Gourrier A, et al. Bone mineral organization at the mesoscale: a review of mineral ellipsoids in bone and at bone interfaces. Acta Biomater. 2022;142:1-13.
55. Alfieri R, Vassalli M, Viti F. Flow-induced mechanotransduction in skeletal cells. Biophys Rev. 2019;11(5):729-743.
56. van Tol AF, Schemenz V, Wagermaier W, et al. The mechanoresponse of bone is closely related to the osteocyte lacunocanalicular network architecture. Proc Natl Acad Sci. 2020;117(51):32251-32259.
57. van Tol AF, Roschger A, Repp F, et al. Network architecture strongly influences the fluid flow pattern through the lacunocanalicular network in human osteons. Biomech Model Mechanobiol. 2020;19(3):823-840.
58. Beno T, Yoon YJ, Cowin SC, Fritton SP. Estimation of bone permeability using accurate microstructural measurements. J Biomech. 2006;39(13):2378-2387.
59. Gatti V, Azoulay EM, Fritton SP. Microstructural changes associated with osteoporosis negatively affect loading-induced fluid flow around osteocytes in cortical bone. J Biomech. 2018;66:127-136.
60. Roschger A, Gamsjaeger S, Hofstetter B, et al. Relationship between the v2PO4/amide III ratio assessed by Raman spectroscopy and the calcium content measured by quantitative backscattered electron microscopy in healthy human osteonal bone. J Biomed Opt. 2014;19(6):65002.